Hindawi
Adsorption Science & Technology
Volume 2021, Article ID 7130581, 11 pages
https://doi.org/10.1155/2021/7130581

Research Article

Efficient Removal of 2,4-DCP by Nano Zero-Valent Iron-Reduced Graphene Oxide: Statistical Modeling and Process Optimization Using RSM-BBD Approach

Qi Jing, Shuo Qiao, Wenyu Xiao, Le Tong, and Zhongyu Ren

Faculty of Architecture, Civil and Transportation Engineering, Beijing University of Technology, Beijing 100124, China

Correspondence should be addressed to Qi Jing; jingqi@bjut.edu.cn

Received 23 August 2021; Revised 24 September 2021; Accepted 12 October 2021; Published 9 November 2021

Academic Editor: Stefano Salvestrini

In this study, nano zero-valent iron-reduced graphene oxide (NZVI-rGO) composites were synthesized to remove 2,4-dichlorophenol (2,4-DCP) as an efficient adsorbent. Scanning electron microscopy (SEM) and X-ray diffraction (XRD) indicated that NZVI particles were successfully loaded and dispersed uniformly on rGO nanosheets. Fourier transform infrared spectroscopy (FTIR) analysis showed that the interaction between NZVI-rGO and 2,4-DCP promoted the adsorption process. A three-level, four-factor Box-Behnken design (BBD) of the response surface methodology (RSM) was used to optimize the influencing factors including NZVI-rGO dosage, 2,4-DCP initial concentration, reaction time and initial pH. A statistically significant, well-fitting quadratic regression model was successfully constructed to predict 2,4-DCP removal rate. The high F value (15.95), very low P value (<0.0001), nonsignificant lack of fit, and appropriate coefficient of determination ($R^2 = 0.941$) demonstrate a good correlation between the experimental and predicted values of the proposed model. The analyses of variance reveal that NZVI-rGO dosage and reaction time have a positive effect on 2,4-DCP removal, whereas the increase of contaminant concentration and initial pH inhibit the removal, whereas the effect of contaminant concentration and initial pH is in reverse, where the change of NZVI-rGO dosage has the greatest effect. The optimum condition is1.215 g/L of NZVI-rGO dosage, 20.856 mg/L of 2,4-DCP concentration, 4.115 of pH, and 8.157 min of reaction time. It is verified by parallel experiments under the optimum condition, achieving the removal efficiency of100%.

1. Introduction

According to recent studies, it is apparent that polluted water is widespread in cities, rural areas, and even in the ocean. Chlorophenols, as an important organic intermediate, are widely used in the synthesis of dyes, leather, fungicides, wood preservatives and phenolic resins, leading to extensive distribution in the aquatic environment [1, 2]. Only a small part of refractory organic matters can be converted into slightly toxic or nontoxic substances by natural degradation, and the rest will migrate in soil and water by volatilization, leaching, and adsorption, posing a continuous threat to human health [3]. The presence of 2,4-DCP (a typical chlorophenol contaminant) in the aquatic environment has attracted the attention of researchers because of its carcinogenic, mutagenic, and hardly biodegradable property [4].

In previous studies, many methods such as adsorption [5], advanced oxidation [6], and photocatalysis [7] have been developed to remove 2,4-DCP. Nano zero-valent iron (NZVI) has been extensively used in the removal of heavy metals [8], dyes [9], antibiotics [10], and various mixed pollutants [11] since it possess excellent properties such as large specific surface area, strong reducibility, and high reactivity [12]. However, there are still some limits of NZVI which affect its large-scale application in practice. Besides the tendency of aggregation caused by magnetic interaction among particles and nanosize effect [13], there is another side that NZVI particles are easy to oxidize when exposed to air [14], which also restrict its application. To overcome these limits, the most common solution adopted is to find apposite modification methods to stabilize and improve dispersion of NZVI particles [15]. Reduced graphene oxide (rGO), a

carbon material that has been developed in recent years, is proved to be effective and promising for the contaminant removal from aqueous media due to its large theoretical specific surface area, extraordinary electrical conductivity, and high surface free-energy [16]. Over the past years, various functionalized graphene materials are used in the field of pollutant removal. For example, synthesizing the composite of graphene and metal materials to remove organic dyes [17], phenolic compounds [18], or explosives [19], combining graphene with polymer to remove heavy metal ions [20] and excessive micronutrient [21], doping with certain elements to remove nitrate [22].

Response surface methodology (RSM), as a statistical and mathematical tool, is used to optimize various factors and estimate the interaction between influencing factors with a limited number of experiments [23]. Selecting an appropriate design strategy has a substantial influence on the precision of the predicted model, such as full factorial design (FFD), central composite design (CCD), and Box-Behnken design (BBD). Unlike CCD that explores a wider range of variables [24], the main advantage of the BBD is to avoid experiments performed under extreme conditions. In this work, the experimental range of independent variables has been determined in advance by batch experiments, so it is not rather necessary to discuss the situation where all factors take extreme values. Finally, RSM based on Box-Behnken design was chosen to construct an experimental model. The independent variables in this study were a dosage of NZVI-rGO, initial 2,4-DCP concentration, reaction time, and initial pH, considering the removal rate of 2,4-DCP as a response value.

In recent years, several studies have confirmed the better efficiency of removing pollutants by NZVI supported on graphene (NZVI-rGO) compared to bare NZVI [25, 26], but there are no researchers that have applied it on the removal of 2,4-DCP. Due to the interaction between NZVI-rGO and 2,4-DCP and the strong adsorption capacity brought by the huge specific surface area of rGO, NZVI-rGO was synthesized to improve the dispersion of nanoparticles and applied for removing 2,4-DCP from the aqueous solution. In this work, the interaction between the factors affecting the removal process is analyzed and the removal behavior is optimized by using RSM-BBD design with considerably less experimental runs. The main aims of this study are (1) to successfully synthesize NZVI-rGO composites and to be characterized by scanning electron microscopy (SEM), X-ray diffraction (XRD), and Fourier transform infrared spectroscopy (FTIR); (2) to apply a four factor, three-level Box-Behnken experimental design to estimate the influence of factors and their interactions on the removal of 2,4-DCP; and (3) to test the validity of the constructed model by a set of parallel experiments in the experimental domain.

Table 1: Independent variables and experimental level in this study.

Independent variable	Factors	Experimental level		
		Low (-1)	Middle (0)	High (+1)
Dosage (g/L)	A	0.5	1.0	1.5
Concentration (mg/L)	B	10	25	40
Reaction time (min)	C	1	5.5	10
pH	D	3	7	11

Table 2: Design matrix with experimental results and predicted values.

Run	*A* g/L	*B* mg/L	*C* min	*D* pH	Experimental %	Predicted %
1	-1	-1	0	0	36.73	38.45
2	-1	0	-1	0	50.44	53.54
3	-1	0	0	-1	9.08	6.10
4	-1	0	0	1	35.31	36.12
5	-1	0	1	0	9.46	6.52
6	-1	1	0	0	18.88	19.17
7	0	-1	-1	0	90.11	86.04
8	0	-1	0	-1	34.97	31.78
9	0	-1	0	1	85.46	83.65
10	0	-1	1	0	39.77	47.22
11	0	0	-1	-1	37.39	42.81
12	0	0	-1	1	90.78	91.03
13	0	0	0	0	78.17	71.84
14	0	0	0	0	73.11	71.84
15	0	0	0	0	69.85	71.84
16	0	0	0	0	72.44	71.84
17	0	0	0	0	65.61	71.84
18	0	0	1	-1	18.08	18.01
19	0	0	1	1	46.56	41.32
20	0	1	-1	0	59.96	63.19
21	0	1	0	-1	35.67	26.61
22	0	1	0	1	53.93	46.25
23	0	1	1	0	12.75	27.51
24	1	-1	0	0	86.97	86.87
25	1	0	-1	0	98.13	90.19
26	1	0	0	-1	36.90	46.78
27	1	0	0	1	74.61	88.28
28	1	0	1	0	76.67	62.70
29	1	1	0	0	65.12	63.58

2. Materials and Methods

2.1. Materials and Instruments. Graphite powder was purchased from Tianjin Guangfu Fine Chemical Industry to prepare graphene oxide (GO). Acid reagents, such as concentrated sulfuric acid (H_2SO_4, 98%) and hydrochloric acid (HCl, 38%), were obtained from Hengfeng Chemical Co., Ltd. Potassium permanganate ($KMnO_4$, Laiyang Fine Chemicals), ferrous sulfate ($FeSO_4{\cdot}7H_2O$, Aladdin), sodium nitrate ($NaNO_3$, Aladdin), sodium borohydride ($NaBH_4$, Aladdin), hydrogen peroxide (H_2O_2, Aladdin), 2,4-dichlorophenol, (2,4-DCP, Macklin biochemical Co., Ltd., GC, >99.7%), and sodium hydroxide (NaOH, Beijing Chemical Works) were all analytical grade. In addition, all solutions

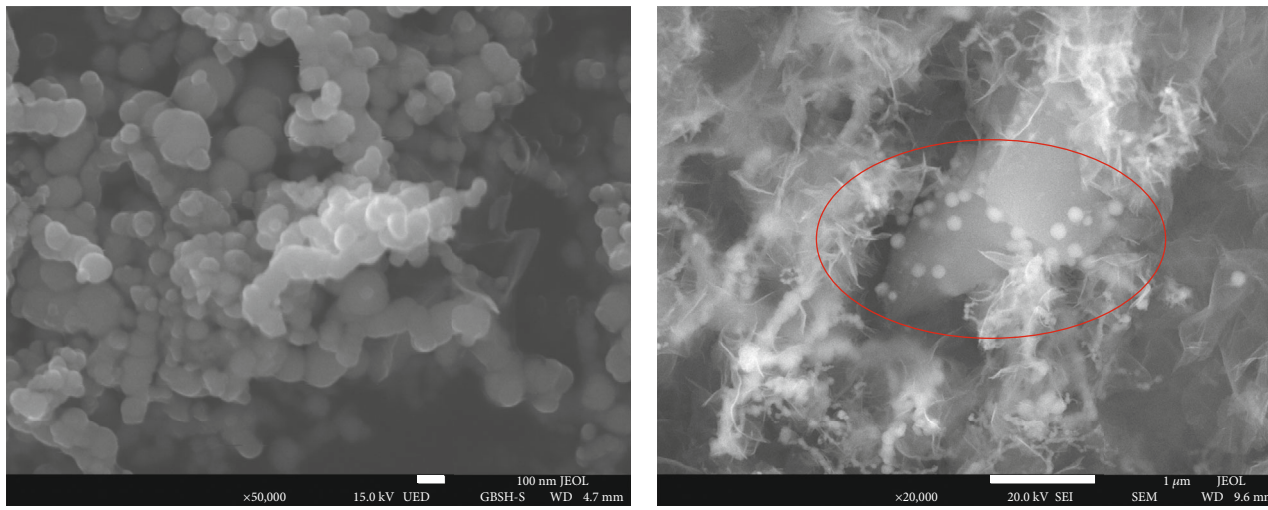

(a) (b)

Figure 1: SEM images of (a) bare NZVI and (b) NZVI-rGO.

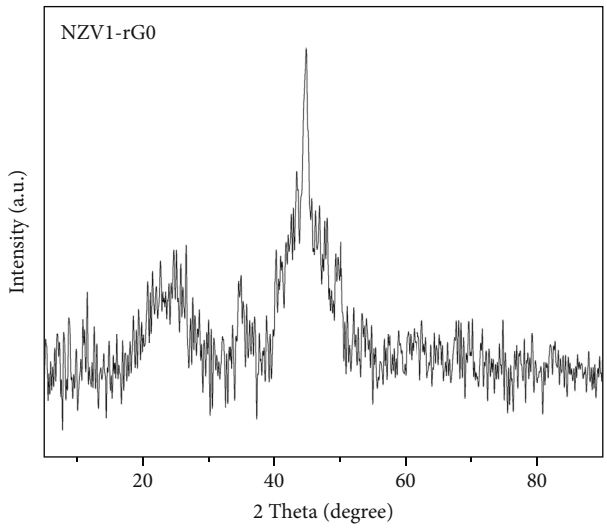

Figure 2: XRD pattern of NZVI-rGO.

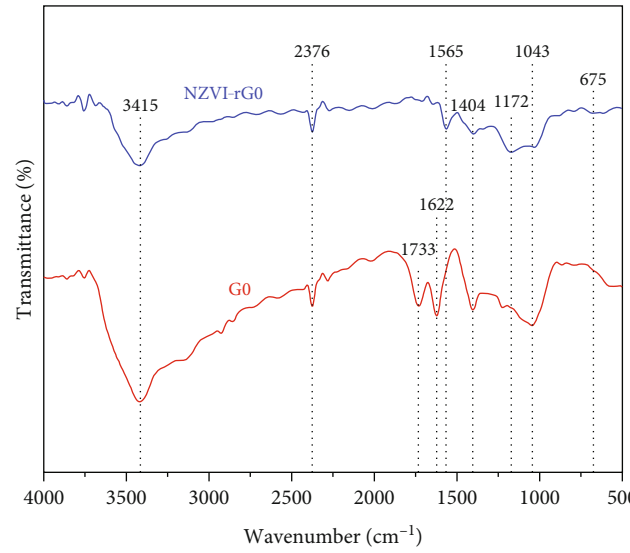

Figure 3: FTIR spectra of the GO andNZVI-rGO.

used in the experiment were prepared with deionized (DI) water from a MX Milli Q system (Fly science, SIM-T30UV).

The concentration of residual 2,4-DCP in a reaction solution was determined by the high-performance liquid chromatography (HPLC, Shimadzu, LC-2030). The parameters for determination of 2,4-DCP concentration are as follows: liquid phase ratio of methanol-water (60 : 40), flow rate 1 mL/min, retention time 13.5 min, injection volume 20 μL, and maximum absorption wavelength of 2,4-DCP 280 nm.

2.2. Synthesis of NZVI-rGO. GO is prepared from graphite powder by modified Hummer's method under the strong oxidation of $KMnO_4$ and H_2SO_4 [27]. As the reaction temperature and time of the second stage are primary factors in the synthesis process, they are assigned to35°C and two hours, respectively. In order to exfoliate GO into nanosheets, 1 g GO was dissolved in 200 mL DI water and decomposed by ultrasonic cell crusher (Biosafer, 900-92) for10 min, then ultrasonicated by water bath for 2 hours. Transfer the above suspension and 50 mL aqueous solution containing 2.482 g $FeSO_4{\cdot}7H_2O$ to a three-necked flask. $Fe^{2+}$and GO were reduced to form NZVI-rGO under the strong reducibility of $NaBH_4$ solution (4.675 g/50 mL) which was dropwise added into the flask at room temperature, and the mixture was continuously stirred for 1 h under N_2 protection to ensure the anaerobic condition. The prepared products were collected by vacuum filtration and washed 2-3 times with DI water. Finally, the black solid was vacuum freeze dried for further use.

2.3. Characterization. The morphology and elemental composition of samples were characterized by using SEM (JSM-7900F, JEOL Ltd., Japan). XRD (Bruker D8 Advance, Germany) with a Cu–Kα excitation source is used to

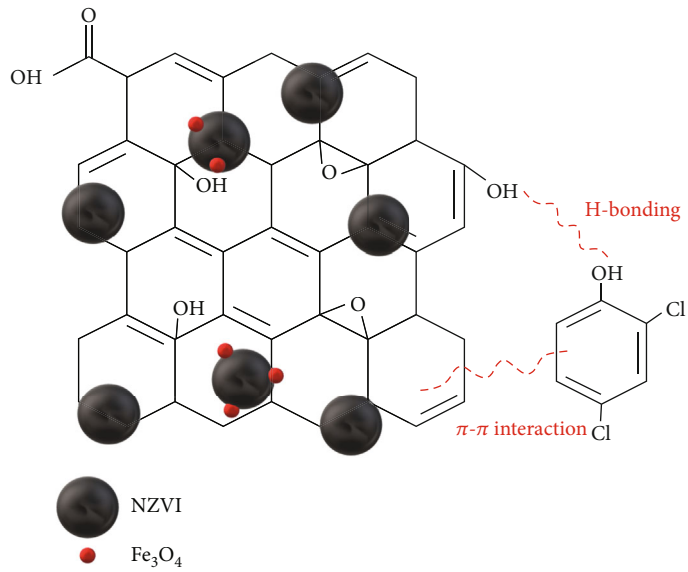

Figure 4: The possible removal mechanisms 2,4-DCP by NZVI-rGO.

investigate the phase composition and crystal structure of NZVI-rGO at 40 kV and 40 mA. The pattern was obtained from 5° to 90°, and the scanning rate was set at about 5° of 2θ/min. Additionally, the functional groups and chemical bonds of the samples were analyzed by FTIR (IRAffinity-1S, Shimadzu, Japan).

2.4. Experimental Design. All experiments were carried out in a water-bath oscillator at a speed of 200 r/min. The experimental range of independent variables was determined by batch experiments (Fig. S1). Water samples were injected into the headspace bottle via 0.45 μm polyethersulfone membrane (PES, Tianjin Jinteng) and sampled at a specific time. The 2,4-DCP removal rate is calculated using Equation (1).

$$2,4-\text{DCP Removal rate}(\%) = \frac{C_0 - C_T}{C_0} \times 100\%, \quad (1)$$

where C_0 and C_T (mg/L) represent the initial 2,4-DCP concentration and the 2,4-DCP concentration at time t (min), respectively. In this study, the RSM based on Box-Behnken design (RSM-BBD) was applied to analyze the independent variables and their interactions. An aquadratic mathematical model was established to optimize the reaction process for removal and achieve the optimum response.

The selected variables (NZVI-rGO dosage (A; g/L), 2,4-DCP initial concentration (B; mg/L), reaction time (C; min), initial pH (D) with their limits for 2,4-DCP removal are given in Table 1. Table 2 shows the design matrix including twenty-four factorial points and five replicates of the central points. The quadratic response model for variables can be described as the following general second-order polynomial equation.

$$\begin{aligned} Y = {} & \alpha_0 + \alpha_1 A + \alpha_2 B + \alpha_3 C + \alpha_4 D + \alpha_{12} AB + \alpha_{13} AC \\ & + \alpha_{14} AD + \alpha_{23} BC + \alpha_{24} BD + \alpha_{34} CD + \alpha_{11} A^2 \\ & + \alpha_{22} B^2 + \alpha_{33} C^2 + \alpha_{44} D^2, \end{aligned} \quad (2)$$

where Y is the predicted removal rate of 2,4-DCP; A, B, C, and D represent independent variables; α_0 is the constant offset term; α_i are linear coefficients; α_{ii} are quadratic coefficients; and α_{ij} represent the interaction coefficients. The absolute value of α can reflect the intensity of the influence on the 2,4-DCP removal rate.

The abovementioned BBD experimental design scheme and subsequent statistical analysis, such as F-test, ANOVA analysis, and residuals analysis, are all obtained by Design expert 12 (version 12.0.3.0).

3. Results and Discussion

3.1. Characterization. Figure 1 demonstrates the structure and surface morphology of the bare NZVI and NZVI-rGO by using SEM. Figure 1(a) shows that the spherical bare NZVI particles randomly connect to each other forming a larger aggregate, which is the essential reason for the decrease of reaction activity, whereas it can easily note that NZVI particles adhere to rGO nanosheets are in a monodisperse state (Figure 1(b)). In addition, it can be found that the particle size of NZVI in NZVI-rGO composites all range from 120 to 150 nm and most of them are around 130 nm. In Figure 1(a), the size distribution of NZVI is extremely nonuniform, some are less than 50 nm, and some even exceed 200 nm, as a result of van der Waals force and magnetic interaction between NZVI particles [28]. These observations imply that rGO can significantly decrease the aggregation of NZVI, thus achieving a relatively large surface

Table 3: ANOVA of the response surface for the quadratic model.

Source	Sum of squares	DF	Mean square	F value	P value (Prob > F)	
Model	18693.01	14	1335.22	15.95	<0.0001	Significant
A (dosage)	6463.52	1	6463.52	77.19	<0.0001	
B (concentration)	1358.94	1	1358.94	16.23	0.0012	
C (reaction time)	3836.33	1	3836.33	45.82	<0.0001	
D (initial pH)	4163.43	1	4163.43	49.72	<0.0001	
AB	4.00	1	4.00	0.0478	0.8301	
AC	32.95	1	32.95	0.3935	0.5406	
AD	95.26	1	95.26	1.14	0.3042	
BC	259.69	1	259.69	3.10	0.1000	
BD	2.45	1	2.45	0.0293	0.8666	
CD	155.13	1	155.13	1.85	0.1950	
A^2	826.20	1	826.20	9.87	0.0072	
B^2	472.34	1	472.34	5.64	0.0324	
C^2	1708.82	1	1708.82	20.41	0.0005	
D^2	346.70	1	346.70	4.14	0.0613	
Residual	1172.24	14	83.73			
Lack of fit	1087.43	10	108.74	5.13	0.0646	Not significant
Pure error	84.81	4	21.20			
Cor total	19865.25	28				

area (Text S1), so as to avoid the rapid oxidation of nanoparticles.

Figure 2 shows the XRD pattern of NZVI-rGO, where a broad peak at 25.01° is attributed to the (002) crystalline plane of rGO and the corresponding interlayer spacing of it is about 0.357 nm as calculated from the Bragg's equation, which is less than the layer spacing of GO reported by Luo et al. [29] owing to the removal of the oxygen-containing functional groups from the carbon sheets. There is an intense and sharp diffraction peak at 44.67° corresponding to the (110) plane in the lattice of NZVI-rGO suggesting successfulreduction of Fe^{2+} by $NaBH_4$. The weak intensity peak at 35.1° is assigned to (311) reflecting Fe_3O_4 crystal facet due to the surface oxidation of NZVI particles [30].

Figure 3 is FTIR spectra of GO and NZVI-rGO describing typical peaks related to different oxygen-containing functional groups. For GO, an intense and broad peak at around 3415 cm^{-1} corresponds to the stretching vibration of O–H groups [19]. The characteristic absorption peaks at 1733, 1622, 1404, and 1043 cm^{-1} are attributed to the stretching vibration of C=O (carboxylic acid and carbonyl moieties), aromatic C=C, carboxy O=C–O, and alkoxy C–O, respectively [19, 31, 32]. It can be observed that the C=O vibration band disappears in NZVI-rGO, and the O-H, carboxy O=C–O and C-O stretching bands are retained but weaken, which is due to the removal of partial of the oxygen-containing functional groups. The 2,4-DCP with aromatic structure presents good adsorption affinities to the benzene rings of rGO by π-π interaction [33]. The hydrogen bond between 2,4-DCP and O-H groups of the remaining oxygen-containing functional groups also promote the adsorption process [34]. The epoxy C=O stretching vibration (1172 cm^{-1}) becomes relatively more obvious due to the decrease of the other oxygen-containing functional groups [31]. In addition, the small vibration observed around 2376 cm^{-1} could ascribe to the CO_2 in the environment [35]. Finally, the weak band at 675 cm^{-1} could be assigned to Fe-O stretching vibrations from Fe_3O_4 nanoparticles [36], which is consistent with the XRD results. These phenomena were in accord with a report by Xing et al. [37], further confirming the successful synthesis of NZVI-rGO. The possible adsorption mechanisms for 2,4-DCP by NZVI-rGO are hydrogen bonding and π-π interaction, as illustrated in Figure 4.

3.2. Response Surface Model Fitting and Variance Analysis. Table 2 exhibits the experimental matrix designed by RSM with the corresponding experimental results and predicted values for 2,4-DCP removal efficiency (%). According to the results, a second-order polynomial equation, which expresses the relationship between the removal efficiency of 2,4-DCP and the four independent variables, can be expressed as follows:

$$Y = 71.84 + 23.21A - 10.64B + 17.88C - 18.63D - 1.00AB + 2.87AC + 4.88AD - 8.06BC + 0.78BD - 6.23CD - 11.29A^2 - 8.53B^2 - 16.23C^2 - 7.31D^2. \quad (3)$$

The influence of the variables on the response value can be indicated by "+" (positive relationship between the

Table 4: Multiple regression consequence of the terms for the quadratic model.

Factor	Coefficient estimate	Effect	Sum of squares	PC
Intercept	71.84			
A dosage	23.21	27.30	6463.52	32.77
B concentration	-10.64	5.74	1358.94	6.89
C reaction time	17.88	16.20	3836.33	19.45
D pH	-18.63	17.59	4163.43	21.11
AB	-1.0000	0.05	4.00	0.02
AC	2.87	0.42	32.95	0.17
AD	4.88	1.21	95.26	0.48
BC	-8.06	3.29	259.69	1.32
BD	0.7825	0.03	2.45	0.01
CD	-6.23	1.97	155.13	0.79
A^2	-11.29	6.46	826.20	4.19
B^2	-8.53	3.69	472.34	2.39
C^2	-16.23	13.35	1708.82	8.66
D^2	-7.31	2.71	346.70	1.76

predicted removal rate and independent variable) and "-" (negative effect between the two above). For the real wastewater with a certain contaminant concentration (factor *B*) and pH (factor *D*), the quadratic polynomial equation (Equation (3)) can be used to predict the optimal dosage, so as to save the cost under the condition of meeting the water quality requirements.

ANOVA is a statistical technique which can be used to validate the adequacy of the model developed and the significance of each variable. R^2, as a coefficient to measure the correlation of regression equation, should be $0 < R^2 < 1$, and the larger values mean the better results. A relatively high value of the R^2 ($R^2 = 0.9410$) and adjusted R^2 value (Adj $R^2 = 0.8820$) were obtained which indicates that the statistical prediction is an approach to the experimental results. Besides, the Adeq Precision (the ratio of the predicted value to the average prediction error) is 12.905 (>4) also confirms that the model has high reliability and precision [38].

F value enhances with the increase of the sum of squares (SS), which implies the significance. of related variables [39]. As revealed from Table 3, the significant *F* value (15.95) and the insignificant value of lack of fit (0.0646) for the quadratic mode prove that the selected model is sufficient to interpret the 2,4-DCP removal process. In addition, *P* values less than 0.05 are also very relevant to prove that the corresponding terms have a significant impact on the 2,4-DCP removal rate. So, it can be concluded that each single factor and the square term of the dose, pollutant concentration, and reaction time have a significant impact. The percent contribution (PC) of each item based on the SS value of the corresponding

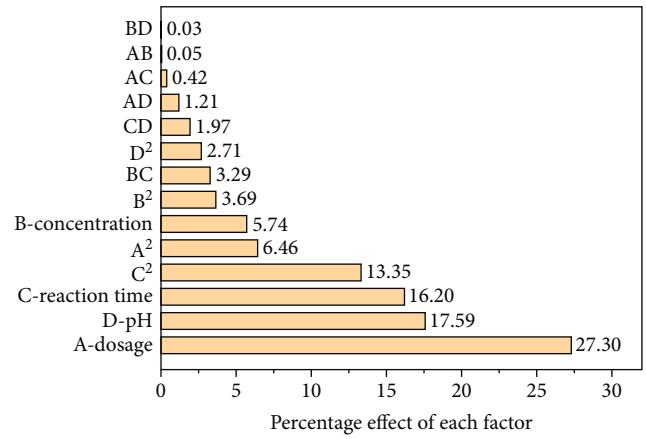

Figure 5: Diagram of Pareto graphic analysis.

term (Table 4) and formula are as follows:

$$\mathrm{PC} = \frac{\mathrm{SS}}{\sum \mathrm{SS}} \times 100. \tag{4}$$

According to the calculation results, the NZVI-rGO dosage shows the most apparent significance with PC near 33and the order of the variable's influence on the removal rate is NZVI-rGO dosage>initial pH>reaction time>2,4-DCP initial concentration.

Figure 5 shows the Pareto graphic analysis which is a method to calculate the percentage influence of each term on the basis of Equation (5) and provides more significant information to explain the results.

$$\mathrm{P_i} = \left(\frac{\alpha_i^2}{\sum \alpha_i^2}\right) \times 100. \tag{5}$$

As can be obtained from the Figure 5, dosage (α_1, 27.30%), pH (α_4, 17.59%), and reaction time (α_3, 16.20%), the quadratic effect of reaction time (α_{33}, 13.35%) produce the main effect on the removal of 2,4-DCP.

3.3. Residual Analysis. To further verify whether the selected model is adequate, the distribution of residuals, predicted values, and actual values are analyzed. Residual analysis is carried out by the virtue of graphic analysis tools, which can be used for the diagnosis of the response surface optimization model [40].

Analyzing the normal plot of residual is an effective way to test the degree of the model fitting. Figure 6(a) depicts the predicted normal residual diagram in which the data points are positioned near an inclined straight line illustrating the residuals have a normal distribution. Figure 6(b) exhibits the studentized residual corresponding to the predicted 2,4-DCP removal efficiency. If the obtained model is reasonable, there should be no evident relativity among the residual and predicted 2,4-DCP removal efficiency [41]. The random distribution of the residuals relative to the zero line indicates that the model is credible. The corresponding residuals of each chronological experiment (shown in Table 2) are presented in

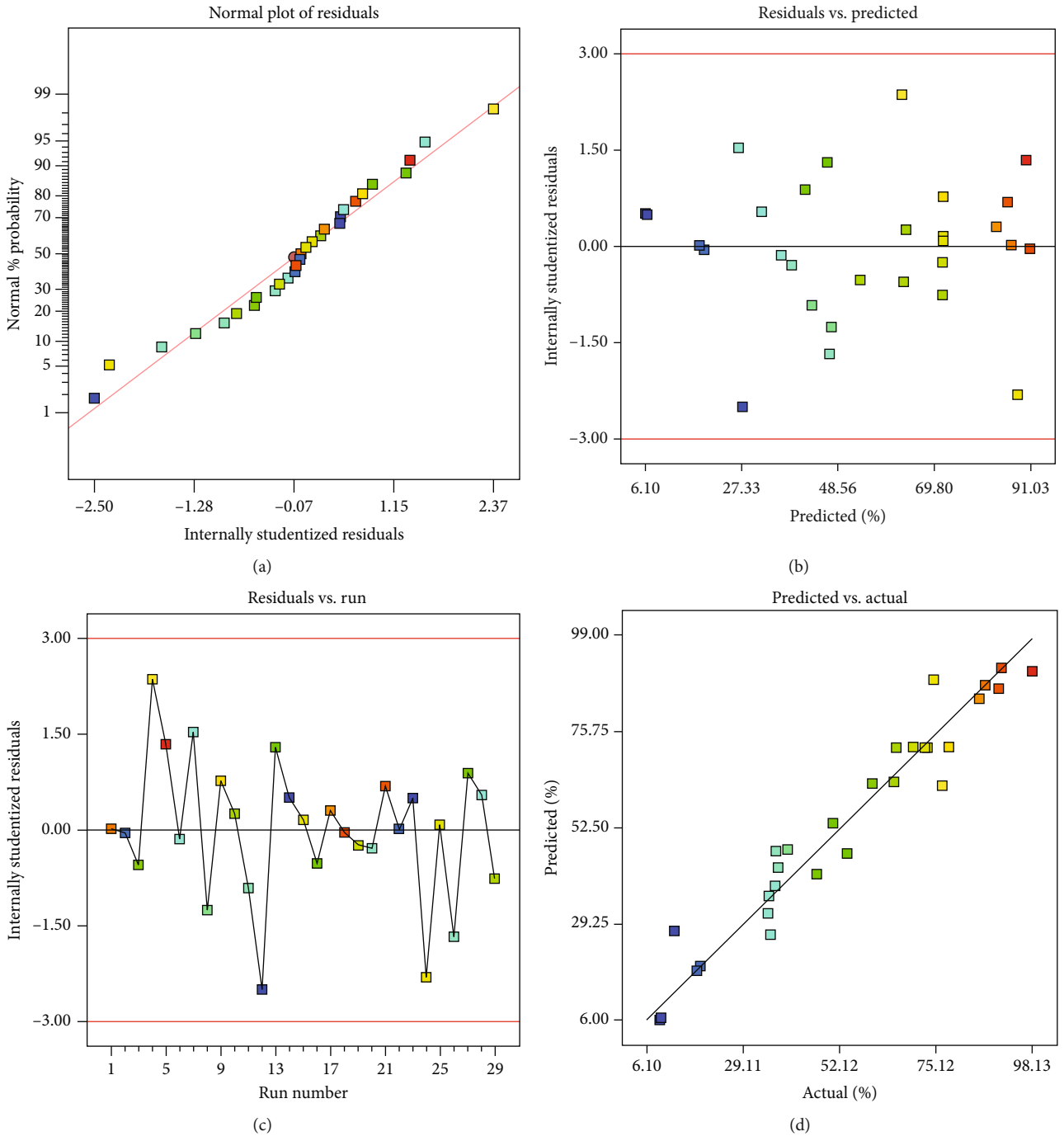

Figure 6: Residual plots for 2,4-DCP removal efficiency by NZVI-rGO. (a) Residuals' normal possibility diagram. (b) Diagram of the residuals based on the predicted value. (c) Chronological diagram of the residuals. (d) Scatter plot of the predicted and actual values.

Figure 6(c). It is found that the residual diagram does not show any specific trend or pattern, which indicates that the hypothesis of experimental conditions is independent guarantying the validity of the experiment [42]. Finally, as shown in Figure 6(d), the outputs calculated by the model are very close to actual 2,4-DCP removal rate signifying the consistency between the two. Therefore, the response surface method has a high degree of confidence in optimizing 2,4-DCP removal from water by NZVI-rGO.

3.4. 3D Response Surface Plots. Figure 7 is the 3D response surface plot which is employed to illustrate the relative influence of two tested variables on the 2,4-DCP removal efficiency while the other two were fixed at the central level. The effects of these factors on the removal of 2,4-DCP are explained via statistical analysis to fit the model and obtain the optimum removal condition.

Figure 7(a) represents the effect of NZVI-rGO dosage and 2,4-DCP initial concentration, when the initial pH and

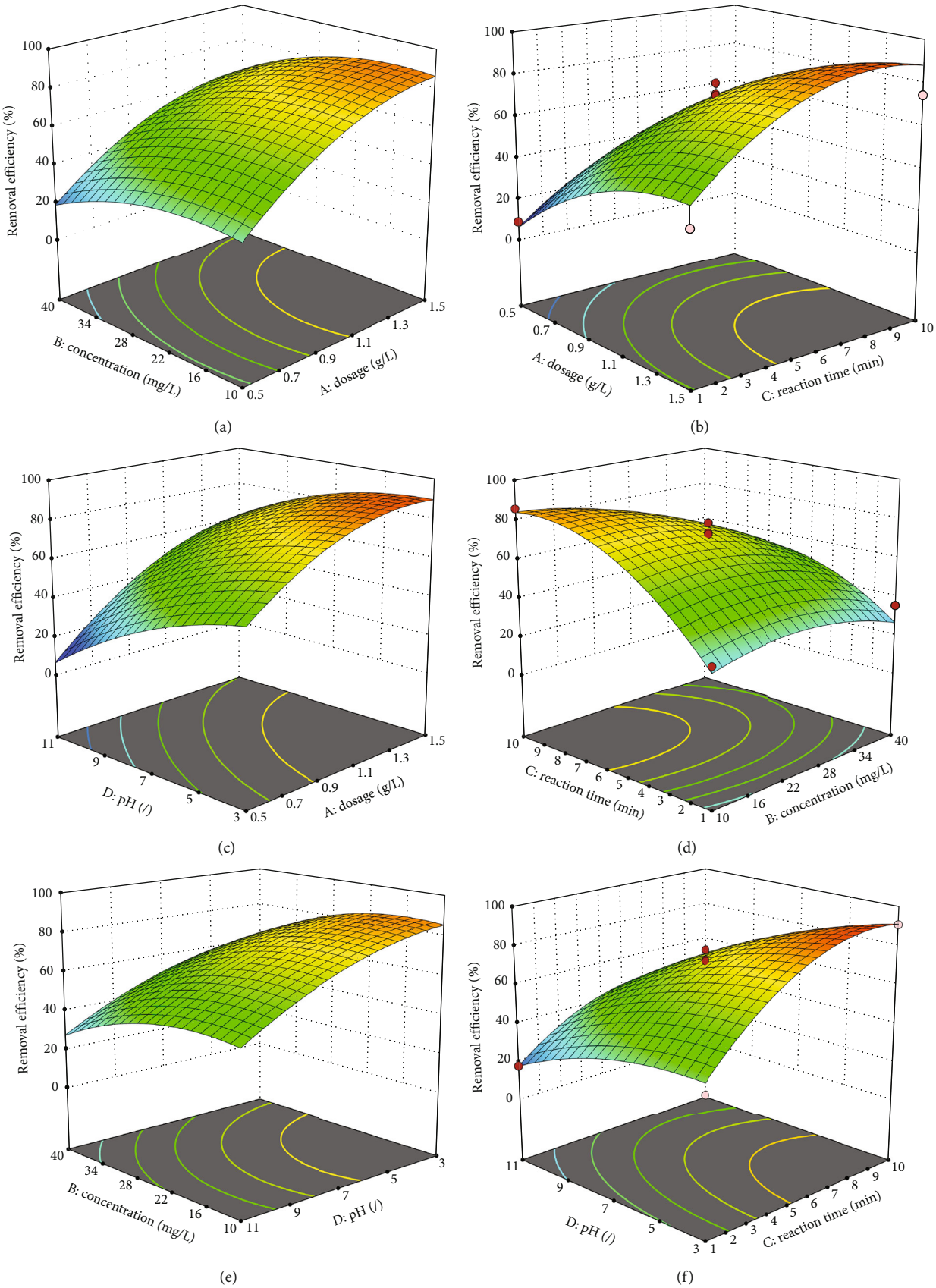

Figure 7: The 3D response surface plots for the (a) dosage and initial concentration, (b) dosage and reaction time, (c) initial pH and dosage, (d) initial concentration and reaction time, (e) initial concentration and initial pH, and (f) initial pH and reaction time.

Table 5: Comparison of the adsorption capacities for 2,4-DCP onto various materials.

Adsorbent	Dosage (g/L)	Q_e (mg/g)	Reaction time (min)	References
NZVI-rGO	1.215	17.17	8.157	This article
Activated carbon	10.00	22.20	360	[44]
Maize cob activated carbons	2.00	17.94	120	[1]
MRGO	0.50	100.00	10	[33]
Bent-nZVI/CTMAB	1.00	32.57	60	[45]
CNT/PI	0.40	506	200	[46]

reaction time were fixed at 7 and 5.5 min, respectively. It is obvious that the adsorbent dosage has positive effects on the removal of 2,4-DCP, whereas the efficiency has no significant variation when the 2,4-DCP concentration is between 10 and 17.5 mg/L and then declines with the increase of concentration. The greater dosage of NZVI-rGO provides more reactive sites and greatly accelerates the transfer of pollutants, which is the key factor to determine the reaction rate which is consistent with the results of variance analysis. The response surface plot for the effect of NZVI-rGO dosage and reaction time on the removal is shown in Figure 7(b), which demonstrates that both of the two factors have a positive impact on the removal of target contaminant. The plot of 2,4-DCP removal affected by NZVI-rGO dosage and initial pH (Figure 7(c)) indicates that the removal rate decreases with the increase of pH value, which is opposite to the trend of dosage. This phenomenon may be due to the inhibition of π-π interaction and cationic-π bond between 2,4-DCP and rGO with the increase of pH value, which leads to the decrease of adsorption capacity at a higher pH value [43]. And the two factors have an evident effect on the 2,4-DCP removal being consistent with the larger F value shown in Table 3.

From Figure 7(d), it is found that the removal rate of 2,4-DCP exhibits a steady but slow decline as the pollutant concentration raised. In the first five minutes, there is almost no difference in the removal rate at different concentrations. With the extension of reaction time, the removal rate will increase slowly. This is due to the composites have enough active sites at the initial stage of the reaction, but when the target pollutants occupy most of the active sites, the competition for adsorption sites among pollutants will lead to the decrease of reaction rate. Finally, Figures 7(e) and 7(f) demonstrate the effect of concentration-initial pH and reaction time-initial pH under the condition that the dosage is 1.0 g/L, respectively. The influence of each factor on the response value is similar with the above results, and there is no apparent interaction between all factors.

3.5. Optimization of Reaction and Model Validation. Using a quadratic model to design the optimal conditions which are carried out from Derringer's desirability function, in order to maximize the removal rate of 2,4-DCP by the nZVI-rGO, the quadratic model was used to optimize all variables within the input range. According to this method, the optimum value of each variable is predicted as dosage of 1.215 g/L, concentration of 20.856 mg/L, pH of 4.115, and reaction time of 8.157 min to reach the maximum removal rate of 100.00%. It is verified by performing three parallel experiments at selected optimum conditions and the result is 100.00%, 100.00%, and 98.73%, respectively. The average relative error between the experimental value and predicted value calculated by the model is 0.43% which verifies the validity of the constructed model in optimization of 2,4-DCP removal process by NZVI-rGO.

The adsorption capability of 2,4-DCP by NZVI-rGO and other adsorbents are exhibited in Table 5. Although the adsorption capacity in this study is relatively low, it has great advantage in shortening the reaction time.

4. Conclusions

In this study, NZVI-rGO was successfully synthesized and shows a brilliant ability for rapidly removing 2,4-DCP from an aqueous solution. A Box-Behnken design was applied to investigate the correlative effects of four independent variables (NZVI-rGO dosage, 2,4-DCP initial concentration, reaction time, and initial pH) on the removal efficiency of 2,4-DCP.

(i) NZVI particles are successfully supported by rGO with a relatively uniform dispersion. The adsorption process is promoted by the virtue of the hydrogen bonding between the oxygen functional groups of NZVI-rGO and 2,4-DCP, π-π interaction between 2,4-DCP and rGO, and the huge specific surface area of rGO

(ii) Analysis of the quadratic model indicates that adsorbent dosage and reaction time have positive effects on the removal efficiency of 2,4-DCP versus the negative effect of 2,4-DCP initial concentration and initial pH, and the change of NZVI-rGO dosage has the greatest effect

(iii) Analysis of variance suggests the high adequacy of the model with high F value (15.95), very low P value (<0.0001), and appropriate coefficient of determination ($R^2 = 0.941$).

(iv) The optimal values of removal conditions were determined as follows: 1.215 g/L of dosage, 20.856 mg/L of 2,4-DCP initial concentration, 4.115 of initial pH, and 8.157 min of reaction time. Under this condition, the predicted removal

efficiency of 2,4-DCP by NZVI-rGO reached100%, which was verified in close agreement with the parallel experimental values (100%, 100%, and 98.73%).

The research findings indicate that NZVI-rGO could be considered a promising adsorbent for the fast and efficient removal of 2,4-DCP from contaminated water.

Data Availability

The data used to support the findings of this study are included within the article.

Conflicts of Interest

The authors have no financial or proprietary interests in any material discussed in this article.

Acknowledgments

We would like to thank all the participants. This study was financially supported by the National Natural Science Foundation of China (Grant No. 41907176).

Supplementary Materials

The supplementary including the "Results of batch adsorption experiments" and "Surface Area Analysis". It is displayed in the document named "Supplementary Files". *(Supplementary Materials)*

References

[1] M. Sathishkumar, A. R. Binupriya, D. Kavitha et al., "Adsorption potential of maize cob carbon for 2,4-dichlorophenol removal from aqueous solutions: equilibrium, kinetics and thermodynamics modeling," *Chemical Engineering Journal*, vol. 147, no. 2-3, pp. 265–271, 2009.

[2] Y. Zhang, O. Haijian, and L. Huixian, "Polyimide-based carbon nanofibers: a versatile adsorbent for highly efficient removals of chlorophenols, dyes and antibiotics," *Colloids and Surfaces A: Physicochemical and Engineering Aspects*, vol. 537, pp. 92–101, 2018.

[3] J.-W.-Y.-M. J. Wan, "Reactivity characteristics of SiO_2-coated zero-valent iron nanoparticles for 2,4-dichlorophenol degradation," *Chemical Engineering Journal*, vol. 221, pp. 300–307, 2013.

[4] J.-P. Wang, F. Hui-Min, and H.-Q. Yu, "Analysis of adsorption characteristics of 2,4-dichlorophenol from aqueous solutions by activated carbon fiber," *Journal of Hazardous Materials*, vol. 144, no. 1-2, pp. 200–207, 2007.

[5] W. Wang, Q. Gong, Z. Chen et al., "Adsorption and competition investigation of phenolic compounds on the solid- liquid interface of three-dimensional foam-like graphene oxide," *Chemical Engineering Journal*, vol. 378, p. 122085, 2019.

[6] T. Lin, L. Yani, and J. Wang, "Enhanced activation process of persulfate by mesoporous carbon for degradation of aqueous organic pollutants: electron transfer mechanism," *Applied Catalysis B: Environmental*, vol. 231, pp. 1–10, 2018.

[7] G. Liao, S. Chen, X. Quan, H. Yu, and H. Zhao, "Graphene oxide modified g-C3N4hybrid with enhanced photocatalytic capability under visible light irradiation," *Journal of Materials Chemistry*, vol. 22, no. 6, pp. 2721–2726, 2012.

[8] G. Liao, S. Chen, X. Quan, H. Yu, and H. Zhao, "High-yield preparation of rod-like CaSO4/Fe0 magnetic composite for effective removal of Cu2+ in wastewater," *Journal of the Iranian Chemical Society*, vol. 13, no. 12, pp. 2185–2191, 2016.

[9] H. Naderpour, N. Meissam, and K.-M. Mozhgan, "Photodegradation of methyl orange catalyzed by nanoscale zerovalent iron particles supported on natural zeolite," *Journal of the Iranian Chemical Society*, vol. 10, no. 3, pp. 471–479, 2013.

[10] Y. Rashtbari, S. Hazrati, A. Azari, S. Afshin, M. Fazlzadeh, and M. Vosoughi, "A novel, eco-friendly and green synthesis of PPAC-ZnO and PPAC-nZVI nanocomposite using pomegranate peel: cephalexin adsorption experiments, mechanisms, isotherms and kinetics," *Advanced Powder Technology*, vol. 31, no. 4, pp. 1612–1623, 2020.

[11] T. Tosco, P. P. Marco, and C. V. Carolina, "Nanoscale zerovalent iron particles for groundwater remediation: a review," *Journal of Cleaner Production*, vol. 77, pp. 10–21, 2014.

[12] Z. Sun, S. Zheng, G. A. Ayoko, R. L. Frost, and Y. Xi, "Degradation of simazine from aqueous solutions by diatomite-supported nanosized zero-valent iron composite materials," *Journal of Hazardous Materials*, vol. 263, pp. 768–777, 2013.

[13] T. Phenrat, N. Saleh, K. Sirk, R. D. Tilton, and G. V. Lowry, "Aggregation and sedimentation of aqueous nanoscale zerovalent iron dispersions," *Environmental Science & Technology*, vol. 41, no. 1, pp. 284–290, 2007.

[14] F. He and Z. Dongye, "Preparation and characterization of a new class of starch-stabilized bimetallic nanoparticles for degradation of chlorinated hydrocarbons in water," *Environmental Science & Technology*, vol. 39, no. 9, pp. 3314–3320, 2005.

[15] M. S. Hasan, M. Geza, R. Vasquez, G. Chilkoor, and V. Gadhamshetty, "Enhanced heavy metal removal from synthetic stormwater using nanoscale zerovalent iron–modified biochar," *Water, Air, & Soil Pollution*, vol. 231, no. 5, 2020.

[16] Z. Pei, L. Li, L. Sun et al., "Adsorption characteristics of 1,2,4-trichlorobenzene, 2,4,6-trichlorophenol, 2-naphthol and naphthalene on graphene and graphene oxide," *Carbon*, vol. 51, pp. 156–163, 2013.

[17] J. Guo, R. Wang, W. W. Tjiu, J. Pan, and T. Liu, "Synthesis of Fe email protected composites for environmental applications," *Journal of Hazardous Materials*, vol. 225-226, pp. 63–73, 2012.

[18] S. Ramanathan, T. Annadurai, and N. Radhika, "Development of rutin-rGO/TiO_2 nanocomposite for electrochemical detection and photocatalytic removal of 2,4-DCP," *Journal of the Iranian Chemical Society*, vol. 18, no. 9, pp. 2457–2472, 2021.

[19] I. K. Bharti, A. K. Shaw, A. Saxena, J. M. Khurana, and P. K. Rai, "Removal of trinitrotoluene with nano Zerovalent iron impregnated graphene oxide," *Water, Air, & Soil Pollution*, vol. 229, no. 1, pp. 1–16, 2018.

[20] H. Jiang, Y. Yang, Z. Lin et al., "Preparation of a novel bioadsorbent of sodium alginate grafted polyacrylamide/graphene oxide hydrogel for the adsorption of heavy metal ion," *Science of the Total Environment*, vol. 744, p. 140653, 2020.

[21] G. Hu, W. Zhang, Y. Chen, C. Xu, R. Liu, and Z. Han, "Removal of boron from water by GO/ZIF-67 hybrid material adsorption," *Environmental Science and Pollution Research*, vol. 27, no. 22, pp. 28396–28407, 2020.

[22] L. Han, B. Li, S. Tao et al., "Graphene oxide-induced formation of a boron-doped iron oxide shell on the surface of NZVI for

enhancing nitrate removal," *Chemosphere*, vol. 252, p. 126496, 2020.

[23] A. Azari, R. Nabizadeh, A. H. Mahvi, and S. Nasseri, "Magnetic multi-walled carbon nanotubes-loaded alginate for treatment of industrial dye manufacturing effluent: adsorption modelling and process optimisation by central composite face-central design," *International Journal of Environmental Analytical Chemistry*, pp. 1–21, 2021.

[24] A. Azari, M. Yeganeh, M. Gholami, and M. Salari, "The superior adsorption capacity of 2,4-Dinitrophenol under ultrasound- assisted magnetic adsorption system: Modeling and process optimization by central composite design," *Journal of Hazardous Materials*, vol. 418, p. 126348, 2021.

[25] A. Masud, N. G. Chavez Soria, D. S. Aga, and N. Aich, "Adsorption and advanced oxidation of diverse pharmaceuticals and personal care products (PPCPs) from water using highly efficient rGO–nZVI nanohybrids," *Environmental science water research & technology*, vol. 6, no. 8, pp. 2223–2238, 2020.

[26] S. Khoshro, M. Naghmeh-Sadat, and S. Samad, "Removal of nitrate from aqueous solution using nano zerovalent iron-reduced graphene oxide composite: optimization of parameters," *Water and environment journal: WEJ*, vol. 34, no. S1, pp. 608–621, 2020.

[27] W. S. Hummers and R. E. Offeman, "Preparation of graphitic oxide," *Journal of the American Chemical Society*, vol. 80, no. 6, p. 1339, 1958.

[28] Y. Zou, X. Wang, A. Khan et al., "Environmental remediation and application of nanoscale zero-valent iron and its composites for the removal of heavy metal ions: a review," *Environmental Science & Technology*, vol. 50, no. 14, pp. 7290–7304, 2016.

[29] M. Xing and J. Wang, "Nanoscaled zero valent iron/graphene composite as an efficient adsorbent for Co(II) removal from aqueous solution," *Journal of Colloid and Interface Science*, vol. 474, pp. 119–128, 2016.

[30] X. Sun, Y. Yan, J. Li, W. Han, and L. Wang, "SBA-15-incorporated nanoscale zero-valent iron particles for chromium(VI) removal from groundwater: Mechanism, effect of pH, humic acid and sustained reactivity," *Journal of Hazardous Materials*, vol. 266, pp. 26–33, 2014.

[31] J. Li, C. Chen, K. Zhu, and X. Wang, "Nanoscale zero-valent iron particles modified on reduced graphene oxides using a plasma technique for Cd(II) removal," *Journal of the Taiwan Institute of Chemical Engineers*, vol. 59, pp. 389–394, 2016.

[32] S. K. Sahoo, S. Padhiari, S. K. Biswal, B. B. Panda, and G. Hota, "Fe3O4 nanoparticles functionalized GO/g-C3N4 nanocomposite: an efficient magnetic nanoadsorbent for adsorptive removal of organic pollutants," *Materials Chemistry and Physics*, vol. 244, p. 122710, 2020.

[33] H. Yan, Q. Du, H. Yang, A. Li, and R. Cheng, "Efficient removal of chlorophenols from water with a magnetic reduced graphene oxide composite," *SCIENCE CHINA Chemistry*, vol. 59, no. 3, pp. 350–359, 2016.

[34] S. Ahmadi, M. Mesbah, C. A. Igwegbe et al., "Sono electrochemical synthesis of LaFeO3 nanoparticles for the removal of fluoride: optimization and modeling using RSM, ANN and GA tools," *Journal of Environmental Chemical Engineering*, vol. 9, no. 4, p. 105320, 2021.

[35] M.-L.-P.-Y. W. Lichun, *The study of CO_2 adsorption on bagasse biochar modified by graphene oxide*, pp. 108–113, 2020.

[36] D. Zhang, Y. Sun, X. Jiang et al., "Assembling nanoscale zero-valent iron on magnetic Fe3O4/reduced graphene oxide composite for efficient reduction of hexanitrohexaazaisowurtzitane (CL-20)," *Desalination and Water Treatment*, vol. 182, pp. 225–236, 2020.

[37] R. Xing, J. He, P. Hao, and W. Zhou, "Graphene oxide-supported nanoscale zero-valent iron composites for the removal of atrazine from aqueous solution," *Colloids and Surfaces A: Physicochemical and Engineering Aspects*, vol. 589, p. 124466, 2020.

[38] Y. Mortezaei, T. Amani, and E. Sh, "High-rate anaerobic digestion of yogurt wastewater in a hybrid EGSB and fixed- bed reactor: Optimizing through response surface methodology," *Process Safety and Environmental Protection*, vol. 113, pp. 255–263, 2018.

[39] R. Oliveira, V. Oliveira, K. K. Aracava, and C. E. da Costa Rodrigues, "Effects of the extraction conditions on the yield and composition of rice bran oil extracted with ethanol–A response surface approach," *Food and Bioproducts Processing*, vol. 90, no. 1, pp. 22–31, 2012.

[40] D. Baş and İ.-H. Boyacı, "Modeling and optimization I: usability of response surface methodology," *Journal of Food Engineering*, vol. 78, no. 3, pp. 836–845, 2007.

[41] M. R. Sohrabi, S. Amiri, H. R. F. Masoumi, and M. Moghri, "Optimization of Direct Yellow 12 dye removal by nanoscale zero-valent iron using response surface methodology," *Journal of Industrial and Engineering Chemistry*, vol. 20, no. 4, pp. 2535–2542, 2014.

[42] U. T. Un, A. Kandemir, N. Erginel, and S. E. Ocal, "Continuous electrocoagulation of cheese whey wastewater: an application of response surface methodology," *Journal of Environmental Management*, vol. 146, pp. 245–250, 2014.

[43] H.-T. Fan, C.-Y. Zhao, S. Liu, and H. Shen, "Adsorption characteristics of chlorophenols from aqueous solution onto graphene," *Journal of Chemical & Engineering Data*, vol. 62, no. 3, pp. 1099–1105, 2017.

[44] M.-Z. Alam, S.-A. Muyibi, and J. Toramae, "Statistical optimization of adsorption processes for removal of 2,4-dichlorophenol by activated carbon derived from oil palm empty fruit bunches," *Journal of Environmental Sciences (China)*, vol. 19, no. 6, pp. 674–677, 2007.

[45] H. Liu, R. Xia, and Z. Dongye, "Enhanced adsorption of 2,4-dichlorophenol by nanoscale zero-valent iron loaded on bentonite and modified with a cationic surfactant," *Industrial & Engineering Chemistry Research*, vol. 56, no. 1, pp. 191–197, 2017.

[46] Q.-L.-Y.-L. H. Yuan and A.-D.-S. Wang, "Preparation of carbon nanotubes/porous polyimide composites for effective adsorption of 2,4-dichlorophenol," *RSC Advances*, vol. 6, no. 98, pp. 95825–95835, 2016.